Int. J. Solids Structures Vol. 29, No. 1, pp. 69–87, 1992
Printed in Great Britain.

0020-7683/92 $5.00 + .00

INFLATION OF AN ELASTIC CYLINDRICAL MEMBRANE: NON-LINEAR DEFORMATION AND INSTABILITY

R. E. KHAYAT, A. DERDOURI and A. GARCIA-RÉJON
Industrial Materials Institute, National Research Council of Canada, 75 De Mortagne Blvd, Boucherville, Québec, Canada J4B 6Y4

(*Received* 22 *October* 1990; *in revised form* 15 *March* 1991)

Abstract—The axisymmetric free inflation of an initially cylindrical membrane is examined in this study. The initial thickness and radius distributions are in general non-uniform. The neo-Hookean constitutive model is used. Special attention is focused on the non-linear buckling instability under various inflation and geometrical conditions. It is found that for a given inflation pressure and aspect ratio S, the thicker the cylinder ends are, the more unstable the deformation becomes. The study also shows that for a given aspect ratio there are in general two solutions and that beyond a maximum S value no solution exists. In some cases of pressure and thickness values the number of bulges increases from one in the unstable cylinder profile as S is increased beyond a certain critical value. A similar phenomenon is observed for a long cylinder when the pressure is increased. Although the problem is formulated to account for non-uniform original thickness and radius distributions, only results based on linear thickness and radius variations are presented.

1. INTRODUCTION

When a rubber cylindrical shell is inflated it becomes unstable at a critical maximum pressure. At this point local bulges may appear in the tube without rupture. If the pressure decreases the size of the bulges may still increase. Some of the early investigations were conducted on an infinite cylinder (Skala, 1970; Alexander, 1971; Erwin *et al.*, 1983; Johnson and Soden, 1966) and a sphere (Green and Adkins, 1960; Haddow and Faulkner, 1972). In these cases an analytical solution to the balance equations is easily obtained for most of the constitutive models commonly used. Skala (1970) correctly predicted the experimentally observed maximum in pressure using a neo-Hookean elastic model. Alexander (1971) also considered the problem of an infinite cylindrical membrane subject to a uniform pressure difference and an axial load. He showed that the critical maximum in pressure remains constant with respect to the imposed axial load when a linear constitutive model is used and it decreases with increasing axial load when a non-linear model is used. While the pressure–radius curves based on both the linear and the non-linear analyses show a maximum, only the non-linear constitutive model leads to a minimum at a larger radius confirming experimental observation. In an attempt to simulate the blowing of polyethylene terephthalate (PET) bottles Erwin *et al.* (1983) used a functional form of the strain energy function suggested by Ward (1971). This constitutive model led to a pressure versus radius behaviour similar to that obtained by Alexander (1971). Similar observations are reached when a spherical membrane is considered (Green and Adkins, 1960; Haddow and Faulkner, 1972). The case of a confined infinite cylinder was tackled by Johnson and Soden (1966) using a neo-Hookean model.

When end effects are included such as during axisymmetric inflation of a finite cylinder the numerical treatment becomes much less tractable. Although the governing equations in this case are ordinary differential equations and therefore amenable to standard numerical solution techniques, the presence of boundary conditions on both ends of the cylinder makes the use of some kind of a shooting procedure imperative. Convergence is by no means guaranteed given the high non-linearities in the equations. Moreover, the presence of stable and unstable solutions for a given driving pressure difference makes it even more difficult to obtain a desired solution in one regime or the other. Similar difficulties are also encountered in the case of a flat membrane (Yang and Feng, 1970; Feng and Huang, 1972; Wineman, 1976, 1978; Charrier *et al.*, 1987, 1989). Benedict *et al.* (1979) considered the

simultaneous inflation and elongation of a finite cylinder subject to an overall axial force. To determine the limiting pressure for a given elongation ratio they implemented the method of projected (pressure) gradient which reduces the search from two dimensions to one. Although the method allows the systematic determination of the maximum in pressure for a given stretch ratio the problems inherent to the (one-dimensional) shooting procedure remain. The special case of zero end forces was first solved by Kydnoiefs and Spencer (1969). This problem is, of course, simpler since only one shooting parameter is involved. The numerical difficulties arising in the case of a cylinder with fixed ends were also anticipated by Petrie and Ito (1980) in their attempt to solve the problem of inflation of a confined cylinder. Only the special case of a flat infinite membrane bounded on two sides was actually considered for calculation. More general discussions on related numerical treatments can be found in the following: Endo *et al.* (1984), Riks (1972, 1979), Chen and Ji (1990), just to name a few. These attempted to devise numerical schemes capable of locating singular points (such as the limit point corresponding to the maximum in pressure or other solution paths in the presence of a bifurcation). Secondary solution paths usually arise for certain values of the parameter(s) involved. These and related questions were addressed by Haughton and Ogden (1979a,b) and Duffett and Reddy (1986) regarding the inflation of finite thin and thick cylinders. Bifurcating solutions are not explored in the present paper and, therefore, will not be discussed any further.

Most of the investigations mentioned above dealt with the question of instability and related numerical difficulties in one way or another. However, actual membrane profiles were seldom determined. The present work attempts to elucidate further on the conditions under which instabilities emerge. Wider ranges of inflation parameters are considered for various values of the aspect ratio and the end thickness of the tube. The formulation is generalised to include non-uniform thickness and radius distributions in the original undeformed state. The strain energy function used in the calculation is that of the neo-Hookean type (Skala, 1970; Kydnoiefs and Spencer, 1969; Petrie and Ito, 1980). This model is known to give qualitatively good agreement with experiment and is simple enough to allow further insight in the non-linear coupling which arises in the governing equations. In fact, comparative studies were carried out using the neo-Hookean and Mooney rubber constitutive equations. It was found that in the case of an infinite cylinder (Skala, 1970), for instance, the Mooney strain function cannot predict the emergence of instability observed beyond the maximum pressure and, instead, leads to a pressure rising to an asymptotic constant value. On the other hand, the case of a finite cylinder (Kydnoiefs and Spencer, 1969) showed that both models give rise to a maximum in the pressure but that only the neo-Hookean model predicts the occurrence of a nearly spherical bulge at the center of the cylinder.

2. PROBLEM FORMULATION

Consider the axisymmetric deformation of an elastic isotropic and incompressible circular cylinder of non-uniform radius and thickness, and length $2L_0$ in the undeformed state. The thickness is assumed to be much less than any radius of curvature; the cylinder is thus regarded as a membrane so that any change in the deformation variables across the thickness may be neglected. Gravity and surface tension effects are neglected. Let (r', ψ', x') be the cylindrical polar coordinates in the deformed configuration with the x' coordinate along the cylinder axis. Note that there is no dependence on ψ because of symmetry. The present notation is similar to that of Petrie and Ito (1980). The original radius and thickness distributions $r_0'(\xi')$ and $h_0'(\xi')$ are imposed functions of the axial coordinate ξ' in the undeformed state. Thus, a material particle currently (after deformation) located at (r', ψ, x') was originally at (r_0', ψ, ξ'). The membrane is allowed to stretch up to a preimposed length $2L$ with the ends of the cylinder located at $x' = 0$ and $x' = 2L$.

For convenience the growing equations and boundary conditions will be formulated in terms of dimensionless quantities. Let

$$r = r'/r_c,$$

$$x = x'/L,$$

$$\xi = \xi'/L, \tag{1}$$

where r_c is a characteristic radial quantity taken to be the value of the cylinder radius at the end. Using these quantities the slope in the longitudinal direction becomes

$$\frac{dr}{dx} = S \tan \theta, \tag{2}$$

θ being the angle between the tangent at (r, ψ, x) and the x-axis, and S the aspect ratio given by $S = L/r_c$. The principal stretch ratios λ_1 and λ_2 are given by

$$\lambda_1 = \frac{ds}{d\xi}, \tag{3}$$

where $s = s'/L$ is the dimensionless arc length along the deformed membrane, and

$$\lambda_2 = \frac{r}{r_0}. \tag{4}$$

The third principal stretch ratio becomes

$$\lambda_3 = \frac{h}{h_0} = \frac{1}{\lambda_1 \lambda_2}, \tag{5}$$

where h and h_0 are the final and initial membrane thicknesses respectively, non-dimensionalised with respect to initial end thickness h_c. Note that eqn (5) results from the incompressibility and conservation of mass conditions. Equation (3) may be rewritten as (Petrie and Ito, 1980):

$$\frac{d\xi}{dx} = \sqrt{\left(\frac{1}{\lambda_1 \cos\theta}\right)^2 - \frac{dr_0}{dx}}. \tag{6}$$

The constitutive equation used in the present calculations is of the hyperelastic type. For an incompressible material ($I_3 = 1$), the strain energy density function can be expressed as

$$W(I_1, I_2) = C_{10}(I_1 - 3) + C_{01}(I_2 - 3)$$

where I_1 and I_2 are the first and second strain invariants, respectively.

In this paper we examine the neo-Hookean model ($C_{01} = 0$). (Skala, 1970; Johnson and Soden, 1966; Kydnoiefs and Spencer, 1969; Petrie and Ito, 1980.) The choice of this particular model is based on its suitability to account (at least qualitatively) for experimental observations (Skala, 1970; Kydnoiefs and Spencer, 1969). Let T'_1 and T'_2 denote the forces per unit length acting in the longitudinal and transverse directions, respectively. The corresponding dimensionless forms of T'_1 and T'_2 are then taken to be

$$T_1 = h(\lambda_1^2 - \lambda_3^2), \tag{7}$$

$$T_2 = h(\lambda_2^2 - \lambda_3^2). \tag{8}$$

Note that T_1 and T_2 are non-dimensionalised with respect to Gr_c. The conservation equations are well known for the present configuration and therefore will not be covered in detail. For variable undeformed thickness and radius one obtains from the conservation of

momentum in the longitudinal and transverse directions the following equations governing Θ and λ_1:

$$\frac{d\theta}{dx} = S\frac{\frac{1}{r}\left(\frac{r}{r_0\lambda_1} - \frac{r_0^3}{r^3\lambda_1^3}\right) - \frac{R_p}{h_0\cos\theta}}{\frac{\lambda_1 r_0}{r} - \frac{r_0^3}{r^3\lambda_1^3}}, \tag{9}$$

$$\frac{d\lambda_1}{dx} = -\frac{S\tan\theta}{r_0}\left(\frac{3r_0^3}{\lambda_1^3 r^3} - \frac{r}{r_0\lambda_1}\right) + \frac{r}{r_0 h_0}$$

$$\times\left[\frac{dh_0}{dx}\left(\frac{\lambda_1 r_0}{r} - \frac{r_0^3}{\lambda_1^3 r^3}\right) + \frac{h_0}{r_0}\left(\frac{\lambda_1 r_0}{r} - \frac{3r_0^3}{\lambda_1^3 r^3}\right)\frac{dr_0}{dx}\right]\left(1 + \frac{3r_0^2}{\lambda_1^4 r^2}\right), \tag{10}$$

where R_p is an inflation parameter given by

$$R_p = \frac{\Delta p r_c}{G h_c} = \frac{\Delta p L}{S G h_c}. \tag{11}$$

with Δp being the imposed inflation pressure. Although λ_1 may be expressed, in general, in terms of the remaining variables as solution to a quartic equation (Kydnoiefs and Spencer, 1969; Petrie and Ito, 1980) eqn (10) turned out to be more convenient to use. On the one hand a quartic equation may possess as many as four possible (real) solutions to select from; in the case of uniform undeformed radius and thickness distributions one can show that only one of the four solutions leads to a positive λ_1 value (Petrie and Ito, 1980). In the present case the choice of a solution branch is far from being obvious. The differential form given by eqn (10) circumvents this difficulty since the physical solution branch is readily adopted once an appropriate boundary condition on λ_1 is imposed. On the other hand, there are some advantages from the computational standpoint when using eqn (10); these will be discussed shortly.

There are four boundary conditions needed for the integration of eqns (2), (6), (9) and (10). For the present problem the radii at the two ends of the cylinder are specified:

$$r(x = 0) = r_1, \tag{12}$$

$$r(x = 2) = r_2. \tag{13a}$$

This latter condition is equivalent to imposing

$$\theta(x = 1) = 0, \tag{13b}$$

in case the deformation is symmetric with respect to the plane perpendicular to the cylinder axis at $x = 1$. If one end of the cylinder, say at $x = 0$, is assumed fixed we have another condition, namely

$$\xi(x = 0) = 0, \tag{14}$$

which states that a particle initially at the left end of the cylinder remains subsequently at that position. There is a variety of options available for the choice of the fourth boundary condition (Feng and Huang, 1972; Wineman, 1976; Kydnoiefs and Spencer, 1969). One may choose to specify the cylinder thickness at the fixed end; this is equivalent to specifying λ_1 at $x = 0$:

$$\lambda_1(x = 0) = \lambda_{10}. \tag{15a}$$

In this case the stretch ratio (ratio of deformed to undeformed lengths), that is $\xi(x = 2)$, will be determined as solution to eqn (6). This particular choice of boundary condition is relevant to inflation processes involving stretching and is extensively investigated in the present work. If a stretch ratio, ξ_2, is imposed the fourth boundary condition becomes

$$\xi(x = 2) = \xi_2. \tag{15b}$$

A special case of interest is when the two ends of the cylinder are held fixed; in this case $\xi_2 = 1$.

3. SOLUTION PROCEDURE

The governing equations (2), (6), (9) and (10) are ordinary first order and non-linear, and are solved subject to conditions (12)–(15). The problem is well-posed and apparently requires no special effort for its numerical solution. There are difficulties, however, arising from two major sources. On the one hand, for a given pressure difference or R_p value one obtains generally two solutions corresponding to stable and unstable deformations (at least in the context of a neo-Hookean model). Therefore beyond a certain maximum R_p value there is no solution. Some kind of an iterative scheme may be used such as the method of projected gradient (Benedict *et al.*, 1987) to determine the maximum pressure difference allowed. On the other hand, not all boundary conditions are specified at one end of the cylinder, for example, at the origin $x = 0$, for an initial-value-problem-type procedure to become readily applicable. If powerful methods such as those of Runge–Kutta or Gear are to be used, an iterative shooting scheme must simultaneously be implemented. Given the non-linear character of the governing equations most shooting techniques are often bound to fail (see, for example, Conte and de Boor, 1972). Indeed, these methods require an initial guess for the variable(s) in question to start the iteration procedure. For a highly non-linear system of equations the guess must be extremely close to the actual variable(s) value(s), thus rendering the method practically useless. One way of avoiding the shooting aspect altogether is to use a finite-difference-type approach. In this case the resulting algebraic (difference) equations governing the discretised variables must be solved simultaneously over the whole domain of computation with the information from both boundaries readily incorporated. However, an initial guess for the discretised variables over the whole domain of calculation is still required to solve the algebraic equations (in this case non-linear) using an iterative solver such as that of Newton–Raphson. This, as will be seen below, may still lead to some problems of stability and convergence inherent to difference schemes.

Current calculations show that no single integration scheme works under all inflation and geometry conditions. The present section aims at elucidating on the different advantages and limitations of the various methods used in the present context. We now examine separately boundary conditions (15a) and (15b). Note that conditions (12)–(14) are assumed always valid. If condition (15a) is assumed to hold, then for a given aspect ratio S, inflation parameter R_p and λ_{10} the stretch ratio ξ_2 will be determined as part of the solution. In this case there is only one shooting condition to consider, namely condition (13) (a or b) at the outer boundary. Thus, one starts integrating the governing equations at $x = 0$ by guessing the value of Θ in an attempt to satisfy condition (13). In principle this should constitute a straightforward numerical exercise which may be carried out using a sixth-order Runge–Kutta integration scheme with a modified Newton–Raphson automatic shooting technique. This latter procedure often failed whenever non-linear effects were pronounced, that is for large R_p value or in the unstable regime. So a *manual* iterative scheme had to be resorted to with no major difficulty except at very small R_p values.

If the stretch ratio ξ_2 is imposed then condition (15b) must hold. The problem becomes that of a two-dimensional shooting procedure which may be extensively tedious to carry out manually; the automatic shooting technique also failed in this case. A variable-step-size-finite-difference procedure was of great assistance in this case despite its initial guess

requirement on the distributions of r, θ, ξ and λ_1 as functions of x. Depending on the initial guess provided the solution may progress towards the stable or unstable branch. Even a marching procedure of updating the initial guess along the pressure–radius curve was not systematic enough when it came to reaching desired stable or unstable solutions. A more convenient way which facilitated the guessing procedure was to actually consider the parameter R_p itself as a dependent variable; in this case we have

$$\frac{dR_p}{dx} = 0. \tag{16}$$

This equation had to be considered together with the set (2), (6), (9) and (10), with the requirement of one additional boundary condition, namely the mid-cylinder radius R_m:

$$r(x = 1) = R_m. \tag{17}$$

The results reported in the next section were obtained for a cylinder symmetric with respect to $x = 1$. The tolerance in the calculations was 10^{-6} with an accuracy of up to the third decimal.

4. NUMERICAL RESULTS AND DISCUSSION

Although the governing equations are formulated to include the cases of non-uniform original thickness and radius in the undeformed state, the emphasis in this study will be on results corresponding to uniform original thickness and radius. The non-uniformity in the original configuration certainly has an influence on the non-linear deformation and deserves further consideration. Several inflation conditions and geometrical configurations were examined:

4.1. *Case* 1: S = 10, λ_{10} = 6 *and* 1.05

We first consider the case of a fixed aspect ratio maintained at $S = 10$. Two separate sets of calculations are carried out for two different cylinder thicknesses. The results for a relatively thin cylinder ($\lambda_{10} = 6$) are presented in Figs 1, 2 and 3. The inflation parameters

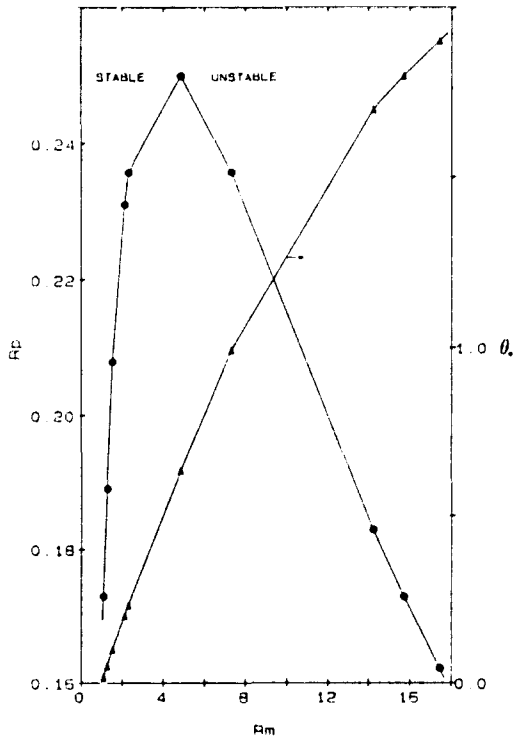

Fig. 1. R_p–R_m and Θ_0–R_m curves for $S = 10$ and $\lambda_{10} = 6$.

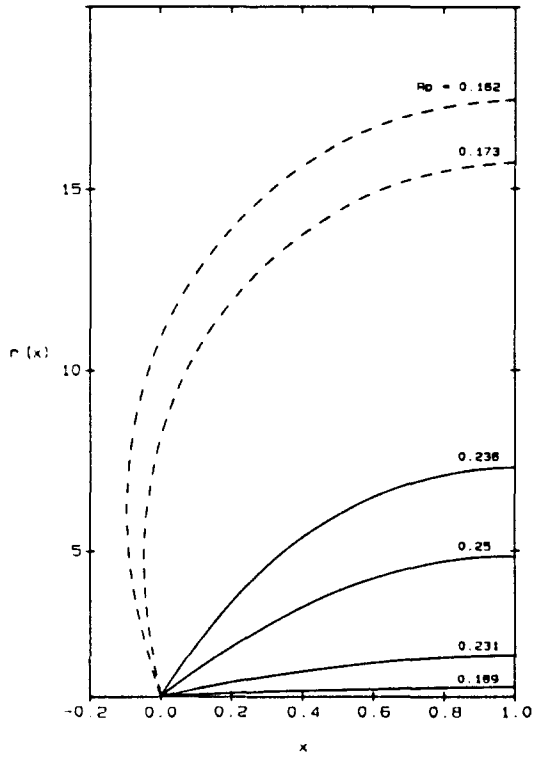

Fig. 2. Stable (——) and unstable (- - -) cylinder profiles for various R_p values, $S = 10$ and $\lambda_{10} = 6$.

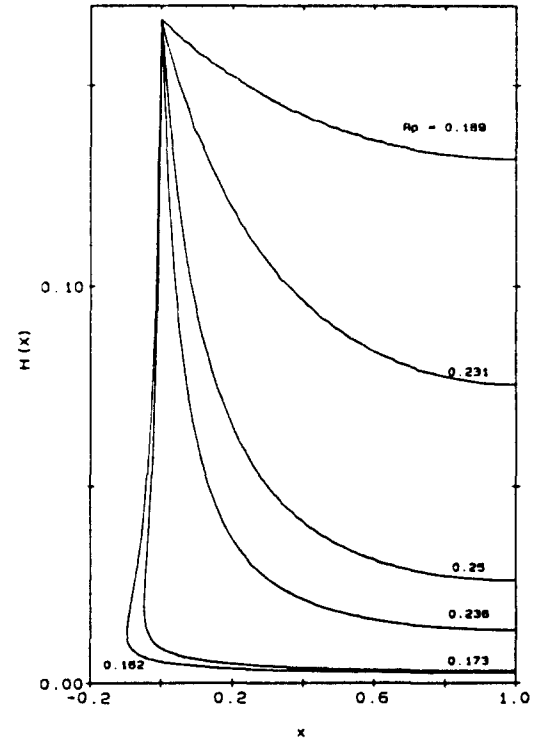

Fig. 3. Thickness distributions for various R_p values, $S = 10$ and $\lambda_{10} = 6$.

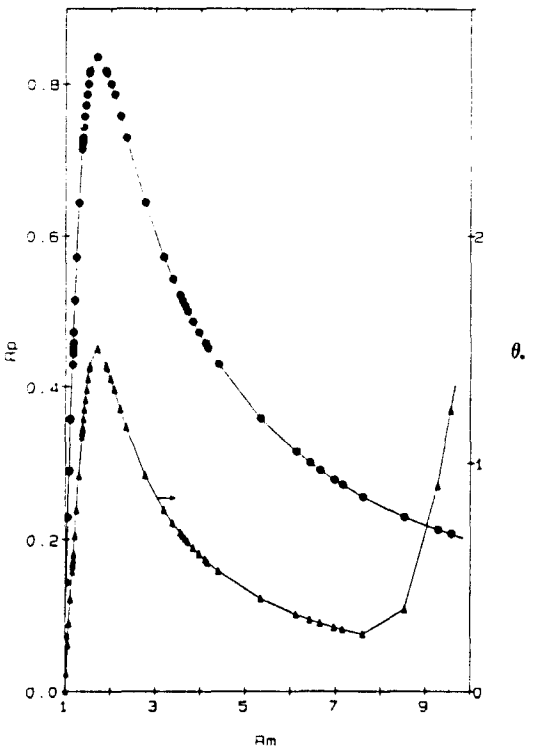

Fig. 4. R_p-R_m and Θ_0-R_m curves for $S = 10$ and $\lambda_{10} = 1.05$.

R_p and Θ_0 are plotted in Fig. 1 as functions of the mid-cylinder radius R_m. Note that R_m is not necessarily the maximum radius, as we will see below. The pressure behaviour exhibits the anticipated maximum separating the stable from the unstable regions while the Θ_0 behaviour shows a monotonic increase with respect to R_m. This latter behaviour may be of some assistance in our attempt to understand the nature of the unstable branch (compare with the Θ_0 curve in Fig. 4). The monotonic increase in Θ_0 reflects the absence of any bulge in the unstable membrane profile. This is confirmed from Fig. 2 where the profiles show the familiar behaviour in both the stable and unstable ranges. The corresponding thickness distributions are shown in Fig. 3. In the stable range the thickness tends to decrease monotonically with respect to the axial position and, as expected, is smallest at the middle of the cylinder. At low pressure, in the unstable regime (curves corresponding to $R_p = 0.162$ and 0.173), the thickness tends to become double-valued with a very steep drop in value near the cylinder end. In the remaining part of the cylinder the thickness is practically constant. It is also interesting to observe that the cylinder thickness tends to decrease generally with increasing pressure in the stable regime in contrast to the unstable regime where it increases when the pressure increases. This of course is due to the large volume that the unstable inflated cylinder tends to occupy in comparison to the stable one (compare, for instance, curves corresponding to $R_p = 0.189$ and 0.162, thus roughly for the same pressure, in both Figs 2 and 3).

For a relatively thick cylinder ($\lambda_{10} = 1.05$) the unstable solution behaviour is fundamentally different from that of the stable one. Figure 4 shows a similar pressure distribution as before with the stable and unstable ranges separated by the maximum in pressure. However, the Θ_0 behaviour now exhibits strong non-monotonicity with respect to R_m. The corresponding cylinder profiles are shown in Fig. 5. In the stable range Θ_0 increases monotonically with respect to R_m reflecting a regular stable inflation as can be depicted from Fig. 5. There is a flattening in the cylindrical membrane almost everywhere except near the end where the cylinder radius increases sharply. At the maximum R_p value, Θ_0 reaches a maximum and starts decreasing like R_p itself when R_m increases. At this stage the cylinder begins to exhibit a bulging part in the middle region with the flat portion gradually receding as the pressure decreases. The emergence of the bulge gives rise to

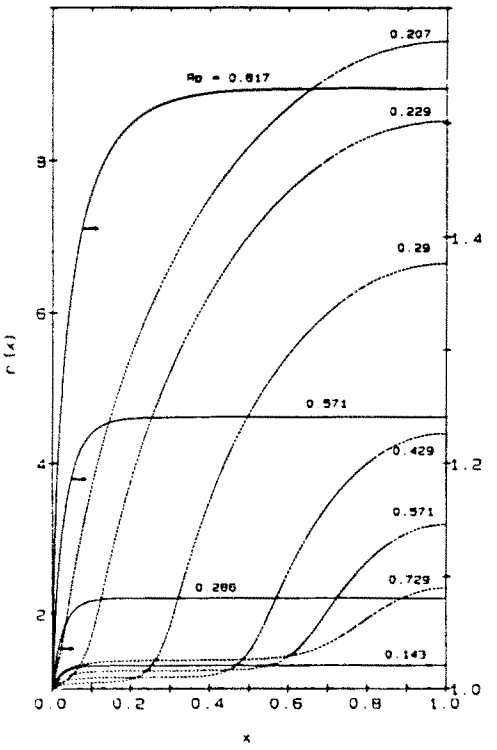

Fig. 5. Cylinder profiles for various R_p values, $S = 10$ and $\lambda_{10} = 1.05$.

compressive stresses in the flat region neighbouring the ends of the cylinder. Since there is no stretching in that region the membrane remains flat. Note that the apparently similar flat portion in the stable profiles do not reflect the presence of compressive forces since the cylinder is undergoing stretching only. As the pressure decreases so does Θ_0; the bulge size increases and the cylinder becomes thinner. Upon further decrease in pressure Θ_0 increases again while the membrane displays similar profiles to those corresponding to the stable branch after the bulge has completely disappeared. One may then conclude from the two studies presented here ($\lambda_{10} = 6$ and 1.05) that a solution in the unstable regime does not necessarily reflect the presence of a bulge or buckling in the cylinder profile. It is also interesting to note that the bulge is present only in the range of R_m between the maximum and minimum Θ_0 in Fig. 4.

4.2. *Case* 2. *The influence of* S

We now examine the influence of the aspect ratio S for various pressures and end thicknesses. Figure 6 displays the mid-cylinder radius R_m as function of S for two inflation parameter values, namely $R_p = 0.173$ and 0.571, and a thickness corresponding to $\lambda_{10} = 6$. It is seen that there is a maximum S value, S_{max}, beyond which no solution exists. The figure shows that S tends to be larger for the lower pressure examined. Thus, the smaller the pressure the more the cylinder has a tendency to stretch. It is also seen that the lower the pressure the more the cylinder tends to grow for a given aspect ratio. The Θ_0 values corresponding to $R_p = 0.173$ show a monotonic increase with respect to R_m. We cannot assert, on the basis of the present steady-state calculations, whether the two branches separated by S_{max} are in fact a stable and an unstable branch, respectively. One cannot, however, exclude such a possibility as will be discussed below. Further insight may be gained by examining the cylinder profiles in Fig. 7 for $R_p = 0.173$. Contrary to the cases of lower λ_{10} values (see below) the present profiles do not exhibit any sign of buckling instability in the membrane at any location and for any aspect ratio.

In the case of a thicker cylinder ($\lambda_{10} = 1.5$ and 1.05) the situation is much more interesting. Figure 8 shows clearly the presence of two branches in the S versus R_m behaviour

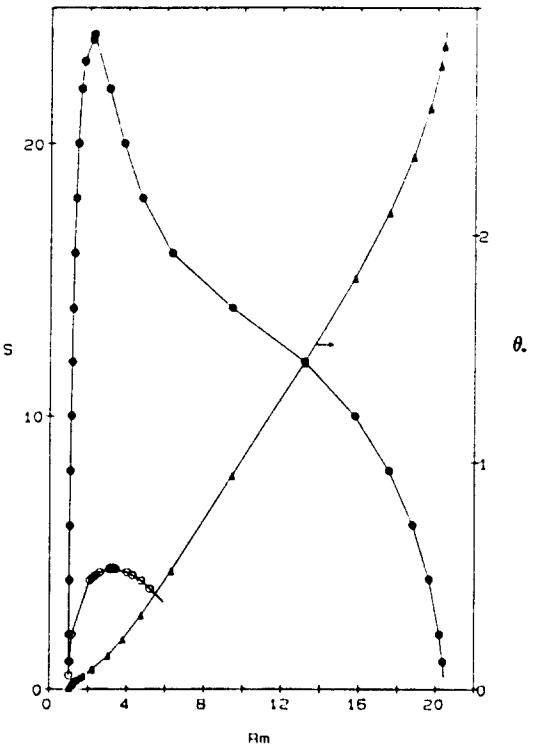

Fig. 6. Dependence of mid-cylinder radius R_m on S for $\lambda_{10} = 6$ (●) $R_p = 0.173$ (○) 0.574. Also shown: Θ_0-R_m curve for $R_p = 0.173$.

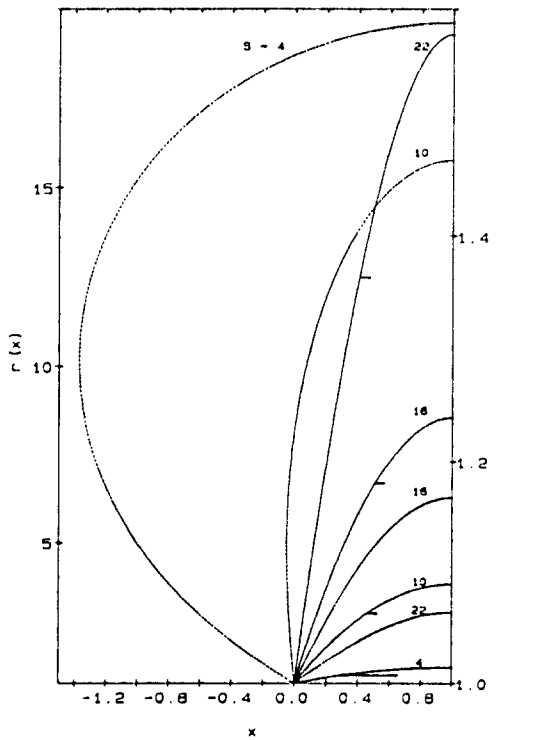

Fig. 7. Stable (——) and unstable (- - -) cylinder profiles for various aspect ratios, $\lambda_{10} = 6$ and $R_p = 0.173$.

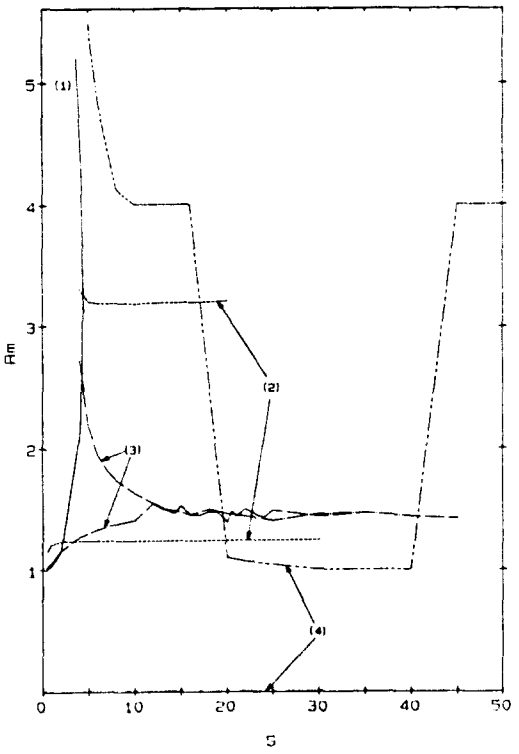

Fig. 8. Dependence of R_m on S for $R_p = 0.571$, $\lambda_{10} = 6$ (curve 1), $\lambda_{10} = 1.05$ (curve 2), $\lambda_{10} = 1.5$ (curve 3), and $R_p = 0.371$, $\lambda_{10} = 1.5$ (curve 4).

corresponding to a given pressure. Generally the two branches do not merge to form a single curve as in Fig. 6. Curves 1, 2 and 3 correspond to $R_p = 0.571$ for $\lambda_{10} = 6$, 1.5 and 1.05, respectively (curve 1 has been reproduced here from Fig. 6 for reference). Our aim is to examine the influence of S for the three thicknesses considered. While curve 1 indicates the presence of a maximum in S, the remaining two exhibit a split between the two branches with R_m becoming constant beyond some S value. The two branches of curve 2 remain separated while in curve 3 they tend to merge with some kind of irregular or oscillatory behaviour. Note that in the latter case it is difficult to tell whether the two branches did indeed merge into a single branch or remained separated. It is to be remembered that the solution procedure is practically incapable of distinguishing a solution to one branch or another and thus may converge almost equally to either one of the two solutions regardless of the initial guess imposed.

The case of $\lambda_{10} = 1.5$ and $R_p = 0.371$ is even more puzzling (curve 4). Here the fluctuation in the R_m value is clearly noticeable. The presence of the second branch is barely detectable since for that relatively low pressure the cylinder remains practically flat. The overall picture becomes much clearer as the actual cylinder profiles are now examined.

The influence of λ_{10} is investigated by examining the cylinder profiles for a given pressure. Figures 9 and 10 display the profiles corresponding to $R_p = 0.571$ for $\lambda_{10} = 0.15$ and 1.05, respectively. For a thinner membrane corresponding to $\lambda_{10} = 6$ the profiles are very similar to those in Fig. 7 and therefore will not be shown; they exhibit a regular behaviour in both the stable and unstable ranges. It is also observed (although not shown) that as S increases the mid-cylinder radius R_m increases in the stable regime whereas the reverse occurs in the unstable regime. Similar behaviour is depicted in Fig. 9 for the thicker cylinder ($\lambda_{10} = 1.5$) except that the unstable cylinder profiles tend to display some waviness for $S > 10$. As the end thickness is further decreased ($\lambda_{10} = 1.05$) the profiles exhibit some fundamental changes in both the stable and the unstable ranges. Indeed, Fig. 10 shows an initial increase in R_m with S, but eventually R_m reaches a constant value for the higher S values with a flattening of the cylinder in the middle region. The flat region tends to occupy

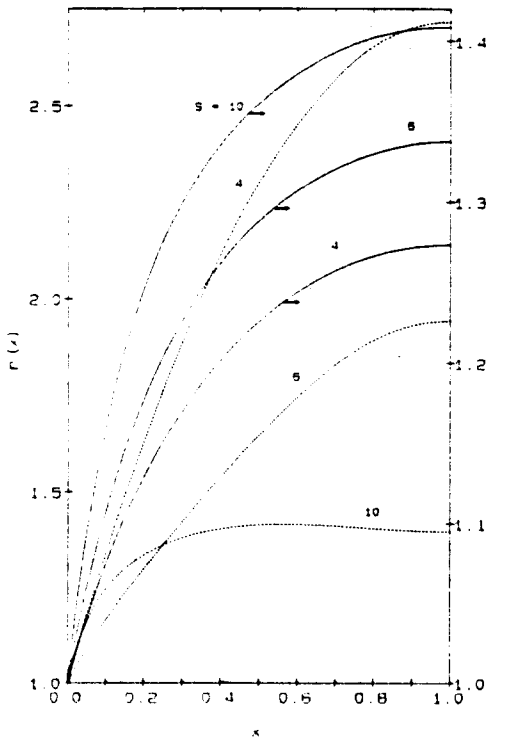

Fig. 9. Stable (——) and unstable (- - -) cylinder profiles for various aspect ratios, $R_p = 0.571$ and $\lambda_{10} = 1.5$.

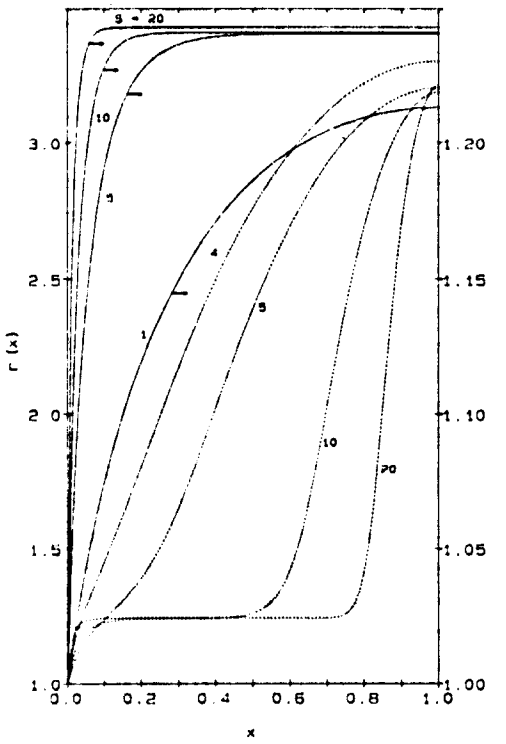

Fig. 10. Stable (——) and unstable (- - -) cylinder profiles for various aspect ratios, $R_p = 0.571$ and $\lambda_{10} = 1.5$.

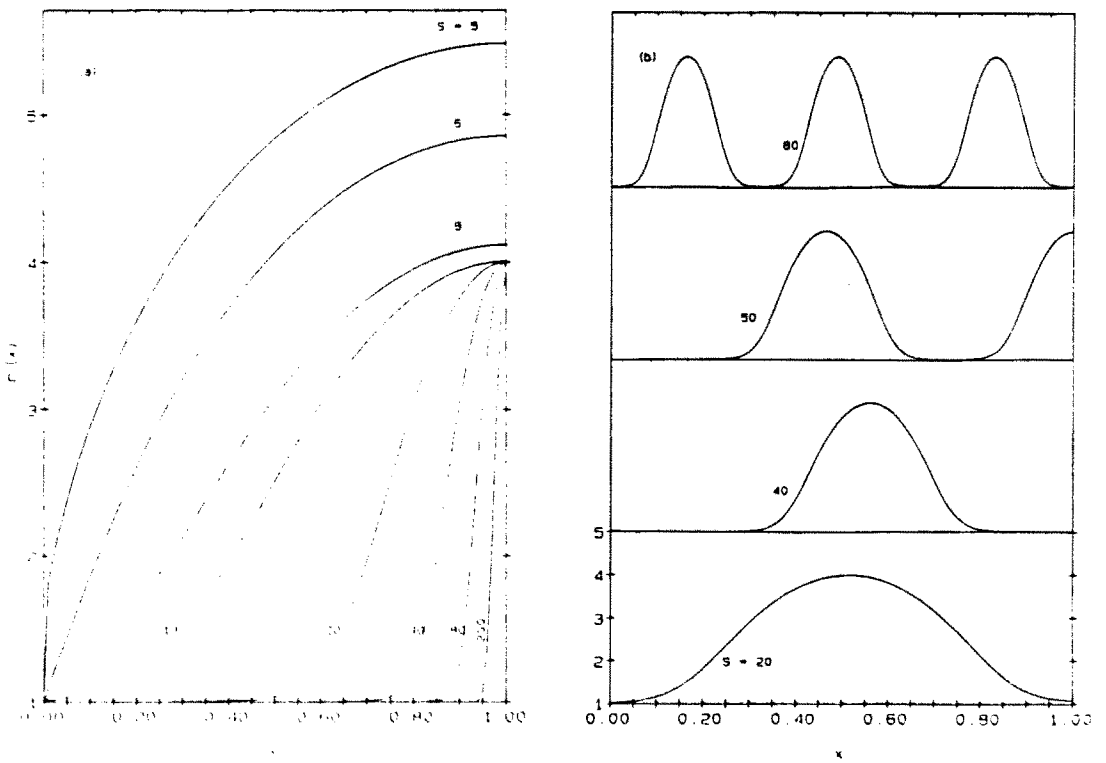

Fig. 11(a). First set of unstable cylinder profiles for various S values, $R_p = 0.371$ and $\lambda_{10} = 1.5$. (b) Second set of unstable cylinder profiles for $R_p = 0.371$ and $\lambda_{10} = 1.5$.

a larger portion of the cylinder length as S increases. Note that the flat part of the cylinder is not undergoing compression as in the case of the unstable range (see below) since a great deal of stretching is taking place near the cylinder ends. In the unstable range the profiles begin to exhibit some buckling instability which becomes more pronounced as S increases. It is interesting to observe from the figure that the compressive flat part between the mid-cylinder region and the ends has a radius higher than the end radius of the cylinder (compare with Fig. 11a).

The case of a relatively low inflation pressure, namely $R_p = 0.371$, leads to some further insight regarding the mechanism of buckling instability. We have seen from Fig. 8 that the corresponding stable branch in curve 4 in the (S, R_m)-plane is practically trivial in the sense that there is barely any (stable) inflation taking place at that pressure. Therefore, one may expect that there remains only one branch to be considered, namely the second branch of curve 4 in Fig. 8 which must be regarded as the unstable range of solutions. It turned out that there is more than just one unstable solution corresponding to a point (S, R_m) of the curve which cannot be detected on the basis of curve 4 alone. Indeed, calculations indicate the existence of a degenerate solution beyond a certain critical value of S (approximately $S_c = 20$ in the present case). The first set of solutions are depicted in Fig. 11a which shows a regular decrease in R_m as S increases and eventually reaches a constant value of $R_m = 4$. It is seen from the figure that for $S < S_c = 20$ the cylinder profiles are regular whereas for $S > S_c$ the profiles begin to exhibit a bulge in the middle of the cylinder which becomes narrower as S increases. Note that in this case the compressive flat portion of the cylinder is at a radius equal to that of the cylinder end (compare with unstable profiles of Figs 5 and 10). The second set of solutions is displayed in Fig. 11b. There does not seem to be any second solution for $S < S_c$. Various numerical procedures and methods were implemented in an attempt to locate a second solution without success. The cylinder profiles exhibit the buckling instability but this time with more than just one bulge along the cylinder. At $S = S_c$ there appears one bulge in the cylinder. Note that due to symmetry only half of the cylinder is shown. As S increases to 30 and 40, the bulge (actually two bulges for the whole cylinder) becomes narrower and its maximum shifts towards the middle

of the cylinder. As S reaches 50 there appears an additional bulge in the middle. Further increase in S (S = 80, 100, 140) gives rise to six bulges in the cylinder. Note that there is practically no change in the value of the maximum radius. Additional calculations show that the number of bulges keeps increasing with S.

4.3. *Case* 3: S = 100 *and* $\lambda_{10} = 1.5$

The calculations presented above evidently show the influence of the aspect ratio on the cylinder profiles and instability. It was particularly found that several bulges may appear in the unstable profiles for a very long cylinder, i.e. when S is large. For this reason it is useful to examine the effect of the inflation parameter for a large aspect ratio, namely $S = 100$. Figure 12 shows the cylinder profiles corresponding to various R_p values and $\lambda_{10} = 1.5$. It is seen from the figure that as R_p increases the buckling instability becomes more evident with an increase in the number of bulges. Note that for a given R_p all the bulges in the profile have the same height and that this height gets larger as the pressure increases. It is also interesting to note that as R_p increases the flat portion of the cylinder between two successive bulges becomes wider, and eventually remains constant or independent of R_p in the higher R_p range where the number of bulges appears to remain equal to four. Obviously some further calculations are needed to be more conclusive.

4.4. *Case* 4: *In the absence of stretch*

We now consider inflation without stretch. In this case eqns (2), (6), (9) and (10) are integrated subject to boundary conditions (12), (13b), (14) and (15b) with $\xi_2 = 1$. As mentioned earlier, this problem involves a two-dimensional shooting procedure and therefore is numerically more difficult (Benedict *et al.*, 1979). A systematic and extensive study as in the previous cases of a cylinder with free ends is of course computationally consuming. We have limited our investigation to three cases of S values, namely S = 5, 10 and 15, and calculated the corresponding R_p, R_m curves as shown in Fig. 13. All three curves show a maximum in pressure separating the stable from the unstable branches. For S = 15 the maximum in pressure is not so well defined as opposed to the two remaining cases. There is a sharp drop in pressure at the maximum (R_m = 1.6) at which point the pressure starts

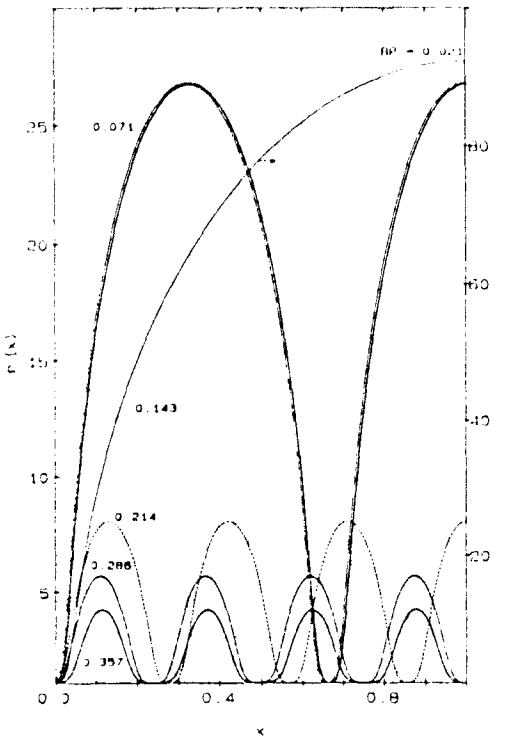

Fig. 12. Unstable cylinder profiles for various R_p values, S = 100 and $\lambda_{10} = 1.5$.

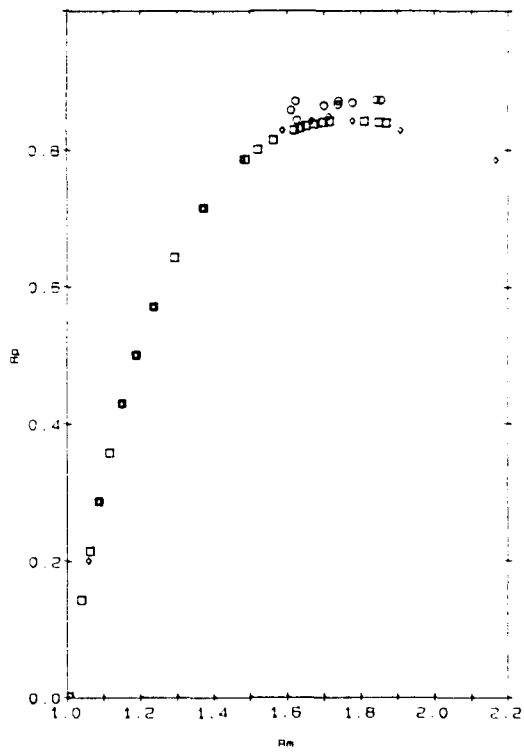

Fig. 13. R_p, R_m curves in the absence of stretch for $S = 5$ (squares), $S = 10$ (diamonds) and $S = 15$ (circles).

increasing again with R_m. The reason for this behaviour becomes clear when the corresponding cylinder profiles are examined. In the low R_m (stable) range the three curves practically coincide for the S values considered. One may then tend to view S as some kind of a similarity parameter and that there exists a universal R_p–R_m curve in the low R_m range. This is certainly not easy to confirm on the basis of the governing equations (2), (6), (9) and (10) and boundary conditions (12), (13b), (14) and (15b).

Some further insight may be gained by examining some of the cylinder profiles. Only those corresponding to $S = 15$ are presented; the two remaining cases exhibit a regular behaviour and therefore will not be shown. It is observed from Fig. 14 that for small R_p values ($R_p = 0.571$ and 0.786) the cylinder remains practically flat except near the ends where there is a sharp increase in radius. As R_p increases the flattening disappears with some buckling ($R_p = 0.854$). For higher R_p values bulges begin to emerge. These bulges, however, are not similar to those arising when stretching is present (see Figs 5, 10–12). In the presence of stretching, the regions in the neighbourhood of the bulges tend to remain flat (and often uninflated) reflecting the presence of compressive forces, whereas in the present case the neighbouring portions to a bulge are expanded.

4.5. *Case* 5: *Non-uniform initial thickness and radius*

We finally examine the influence of the original thickness and/or radius non-uniformity on the deformed cylinder. Calculations were carried out for linear thickness and radius variations with respect to initial position. Figure 15 shows the effect of thickness variation in the stable and unstable regimes, respectively, for two original slopes (the uniform thickness case is included for reference). The stable solution shows an important inflation of the cylinder near the end ($x = 0$) compared to the one in the middle ($x = 1$). It is also observed from the figure that the steeper the original thickness variation, the less the cylinder tends to inflate. The corresponding unstable solutions are somewhat surprising. The figure shows that, the larger the slope in the original (undeformed) thickness the higher the mid-cylinder bulge becomes. A similar but opposite effect occurs when the initial radius increases linearly with position as can be observed from Fig. 16. The stable solution shows a final

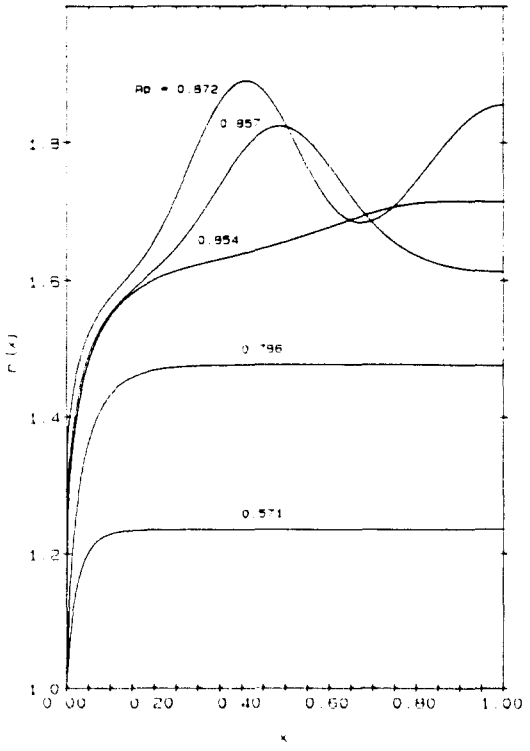

Fig. 14. Cylinder profiles in the absence of stretch for various R_p values and $S = 15$.

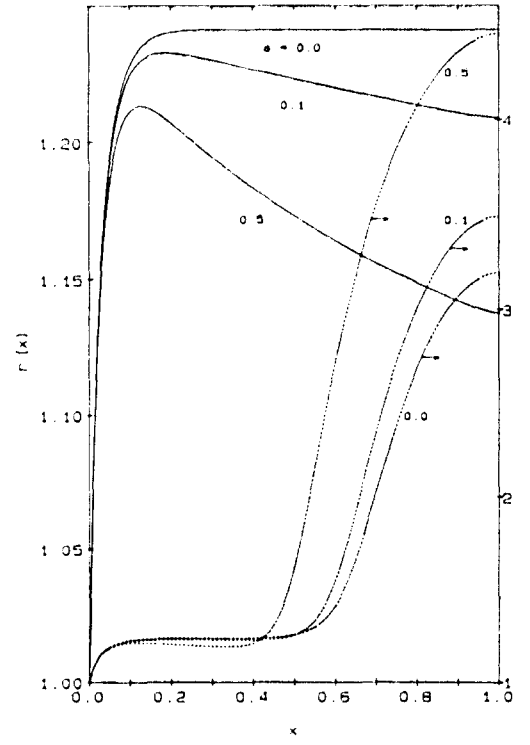

Fig. 15. Stable (——) and unstable (- - -) cylinder profiles for three different slopes (a) in initial thickness variation with $R_p = 0.571$, $S = 10$ and $\lambda_{10} = 1.05$.

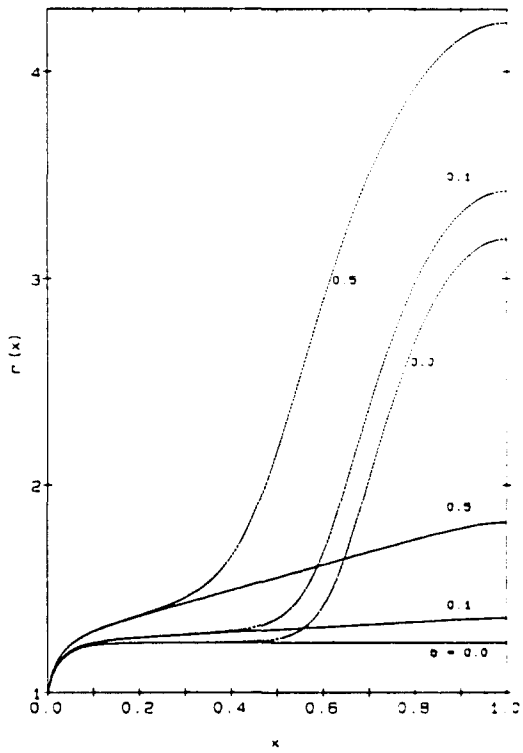

Fig. 16. Stable (——) and unstable (– – –) cylinder profiles for three different slopes (b) in initial radius variation with $R_p = 0.571$, $S = 10$ and $\lambda_{10} = 1.05$.

radius increasing as a function of the initial radius. The unstable solution exhibits the reverse effect. When both the initial thickness and radius increase linearly with position the resulting profiles and thickness distributions are shown in Fig. 17. In this case the effect on the deformed cylinder due to the variation in initial thickness is counter-balanced by that due to the variation in initial radius. Compare the (stable) radius distributions of Fig. 17 to those of Fig. 15. Clearly, the cylinder in the former case tends to inflate less than in the latter case due to the additional effect of initial thickness. Similar arguments apply to the rest of the unstable profiles.

5. CONCLUSION

In this work the balance equations are derived for an elastic solid continuum. The governing equations are generalized to include variable initial thickness and radius in the undeformed state. The resulting equations are bulkier to handle than when the thickness and radius are originally uniform, with the original degree of non-linearity remaining unchanged. Although various techniques have been developed for the numerical solution of the problem, the presence of two boundaries, as we observed, requires the use of a shooting procedure which often failed given the non-linearity of the governing equations. The problem becomes particularly difficult when more than one shooting parameter is involved. In this case a finite-difference integration procedure can be more adequate than an initial-value-problem numerical solver such as Runge–Kutta. However, problems of stability and convergence inherent to the finite-difference scheme can easily arise because of the non-linearities. There is therefore no simple answer to these difficulties and a combination of more than just one integration and one shooting scheme must be resorted to in our attempt to obtain the stable and unstable inflation profiles. The present calculations are carried out using finite-difference and sixth-order Runge–Kutta integration procedures and a modified Newton–Raphson shooting scheme with the latter.

The numerical calculations show that the unstable solution does not always exhibit the presence of a bulge in the deformed cylinder. We first examined the influence of the

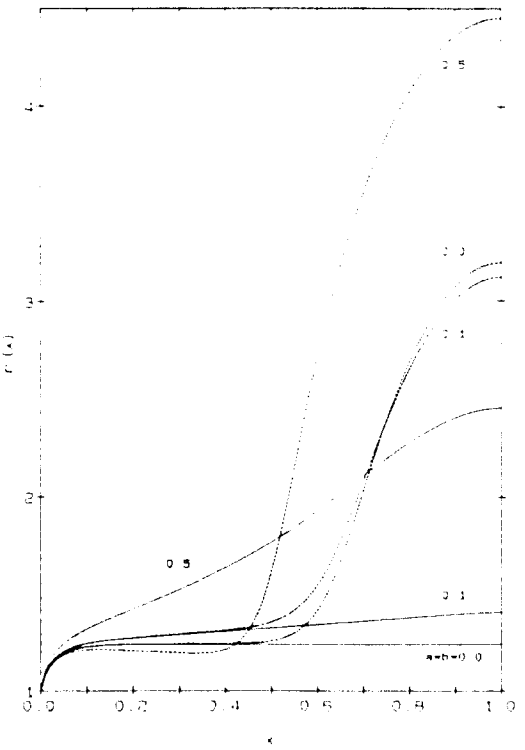

Fig. 17. Stable (——) and unstable ( ) cylinder profiles for three different slopes in initial thickness and radius variations with $R_p = 0.571$, $S = 10$ and $\lambda_{10} = 1.05$.

thickness at the ends of the cylinder on the deformed profiles. When the cylinder ends are relatively thin there is no bulge in the cylinder profiles (Fig. 2). For thicker ends the bulge in the cylinder becomes evident (Fig. 5) and its height increases as the inflation pressure decreases. The influence of the aspect ratio S has also been investigated. It is observed that, for a given pressure, there exists a critical aspect ratio beyond which a bulge begins to appear in the unstable profile. The bulge is found to become narrower the larger the aspect ratio, that is the longer the cylinder (Fig. 11a). Moreover, a second set of solutions shows that the number of bulges increases as S increases (Fig. 11b). Thus, long cylinders tend to allow several bulges in their unstable inflation mode. The number of bulges may also increase when the inflation pressure itself is varied (Fig. 12). This is also particular to long cylinders. Finally we examined the influence of undeformed thickness and/or radius (linear) variation on the inflated cylinder. The resulting stable and unstable profiles exhibited exactly opposite behaviours. For instance, for a variable initial thickness, the stable solution showed a pronounced growth in cylinder radius where the membrane was originally thinnest, whereas the unstable profile gave rise to a bulge where the cylinder was originally thickest (see Fig. 15).

Although extensive work has been previously carried out to determine instability conditions for inflated structures, actual calculations such as the ones presented here are scarce. It is obvious, from the present investigation, that there remains a wide range of other constitutive models, inflation conditions and geometries which must be considered if further understanding of the non-linear buckling were to be achieved. For instance, based on a comparative study conducted on the neo-Hookean and Mooney models (Kydnoiefs and Spencer, 1969) it was found that only the former model gave rise to a bulge in the unstable profiles. Thus, since the present calculations are based on the neo-Hookean constitutive model for the free inflation of a rubber thin cylinder, the results above are likely to be altered if a constitutive model such as Mooney's is adopted. Another interesting aspect which may be given further consideration is the emergence of several bulges along the inflated cylinder. It would be desirable, for instance, to determine a wider range of critical R_p and S values beyond which the number of bulges increases. One may also examine the

effect of non-linear variations of thickness and radius in the undeformed state on the final cylinder profiles. These considerations will undoubtedly require extensive calculations which in turn may not be all that obvious given the numerical difficulties discussed above.

REFERENCES

Alexander, H. (1971). The tensile instability of an inflated cylindrical membrane as affected by an axial load. *Int. J. Mech. Sci.* **13**, 87–95.

Benedict, R., Wineman, A. and Yang, W. H. (1979). The determination of limiting pressure in simultaneous elongation and inflation of non-linear elastic tubes. *Int. J. Solids Structures* **15**, 241–249.

Charrier, J. M., Shrivastava, S. and Wu, R. (1987). Free and constrained inflation of elastic membranes in relation to thermoforming—axisymmetric problems. *J. Strain Anal.* **22**, 115–125.

Charrier, J. M., Shrivastava, S. and Wu, R. (1989). Free and constrained inflation of elastic membranes in relation to thermoforming—non-axisymmetric problems. *J. Strain Anal.* **24**, 55–74.

Chen, Z. Q. and Ji, X. (1990). A new approach to finite deformation problems of elastoplasticity—boundary element analysis method. *Comp. Meth. Appl. Mech. Engng* **78**, 1–18.

Conte, S. D. and de Boor, C. (1972). *Elementary Numerical Analysis: An Algorithmic Approach* (2nd Edn). McGraw-Hill, New York.

Duffett, G. A. and Reddy, B. D. (1986). The solution of multi-parameter systems of equations with application to problems in nonlinear elasticity. *Comp. Meth. Appl. Mech. Engng* **59**, 179–213.

Endo, T., Oden, J. J., Becker, E. B. and Miller, T. (1984). A numerical analysis of contact and limit-point behaviour in a class of problems of finite elastic deformation. *Comput. Struct.* **18**, 899–910.

Erwin, L., Pollock, M. A. and Gonzalez, H. (1983). Blowing of oriented PET bottles: prediction of free blown size and shape. *Polym. Engng Sci.* **23**, 826–829.

Feng, W. W. and Huang, P. (1972). On the inflation of plane non-linear membrane. *J. Appl. Mech.* **41**, 767–771.

Green, A. E. and Adkins, J. E. (1960). *Elastic Deformation and Non-linear Continuum Mechanics*. Clarendon Press, Oxford.

Haddow, J. B. and Faulkner, M. A. (1972). A note on the finite elastic inflation of a thin spherical shell. *Trans. CSME* **1**, 158–160.

Haughton, D. M. and Ogden, R. W. (1979a). Bifurcation of inflated circular cylinders of elastic material under axial loading—I. Membrane theory for thin-walled tubes. *J. Mech. Phys. Solids* **27**, 179–212.

Haughton, D. M. and Ogden, R. W. (1979b). Bifurcation of inflated circular cylinders of elastic material under axial loading—II. Exact theory for thin-walled tubes. *J. Mech. Phys. Solids* **27**, 489–512.

Johnson, W. and Soden, P. D. (1966). The discharge characteristics of confined rubber cylinders. *Int. J. Mech. Sci.* **8**, 213–225.

Kydoniefs, A. D. and Spencer, J. M. (1969). Finite axisymmetric deformations of an initially cylindrical elastic membrane. *Q. J. Mech. Appl. Math.* **22**, 87–95.

Petrie, C. J. S. and Ito, K. (1980). Prediction of wall thickness of blow moulded containers. *Plastics and Rubber: Processing*, June 1980, 68–72.

Riks, E. (1972). The application of Newton's method to the problem of elastic stability. *J. Appl. Meth.* **39**, 1060–1066.

Riks, E. (1979). An incremental approach to the solution of snapping and buckling problems. *Int. J. Solids Structures* **15**, 529–551.

Skala, D. P. (1970). Modified equations of rubber elasticity applied to the inflation mechanics of a thick-walled rubber cylinder. *Rubber Chem. Tech.* **43**, 745–757.

Ward, I. M. (1971). *Mechanical Properties of Solid Polymers*. Wiley, Chichester.

Wineman, A. S. (1976). Large axisymmetric inflation of a non-linear viscoelastic membrane by lateral pressure. *Trans. Soc. Rheol.* **20**, 203–225.

Wineman, A. S. (1978). On axisymmetric deformations of non-linear viscoelastic membranes. *J. non-Newt. Fluid Mech.* **4**, 249–260.

Yang, W. H. and Feng, W. W. (1970). On axisymmetrical deformation of non-linear membranes. *J. Appl. Mech.* **37**, 1002–1011.